Subduction of the oceanic Hikurangi Plateau and its impact on the Kermadec arc

Christian Timm[1], Bryan Davy[1], Karsten Haase[2], Kaj A. Hoernle[3], Ian J. Graham[1], Cornel E.J. de Ronde[1], Jon Woodhead[4], Dan Bassett[5], Folkmar Hauff[3], Nick Mortimer[6], Hannu C. Seebeck[1], Richard J. Wysoczanski[7], Fabio Caratori-Tontini[1] & John A. Gamble[8]

Large igneous province subduction is a rare process on Earth. A modern example is the subduction of the oceanic Hikurangi Plateau beneath the southern Kermadec arc, offshore New Zealand. This segment of the arc has the largest total lava volume erupted and the highest volcano density of the entire Kermadec arc. Here we show that Kermadec arc lavas south of $\sim 32°S$ have elevated Pb and Sr and low Nd isotope ratios, which argues, together with increasing seafloor depth, forearc retreat and crustal thinning, for initial Hikurangi Plateau—Kermadec arc collision $\sim 250\,km$ north of its present position. The combined data set indicates that a much larger portion of the Hikurangi Plateau (the missing Ontong Java Nui piece) than previously believed has already been subducted. Oblique plate convergence caused southward migration of the thickened and buoyant oceanic plateau crust, creating a buoyant 'Hikurangi' mélange beneath the Moho that interacts with ascending arc melts.

[1] GNS Science, PO Box 30-368, Lower Hutt 5040, New Zealand. [2] Geozentrum Nordbayern, Universität Erlangen-Nürnberg, Schlossgarten 5, 91054 Erlangen, Germany. [3] GEOMAR Helmholtz Centre for Ocean Research, FB4, Wischhofstrasse 1-3, 24148 Kiel, Germany. [4] School of Earth Sciences, University of Melbourne, Parkville, Victoria 3010, Australia. [5] Department of Earth Sciences, University of Oxford, Oxford OX1 3AN, UK. [6] GNS Science, Private Bag 1930, Dunedin 9054, New Zealand. [7] National Institute of Water and Atmospheric Research, Private Bag 14901, Wellington 6241, New Zealand. [8] School of Geography, Environment and Earth Sciences, Victoria University of Wellington, PO Box 600, Wellington 6140, New Zealand. Correspondence and requests for materials should be addressed to C.T. (email: c.timm@gns.cri.nz).

The formation of large igneous provinces (LIPs) represents one of the most extreme volcanic events on Earth, characterized through eruption of vast amounts of lava in a geologically short period[1]. Oceanic LIPs either accrete and obduct, adding to the continental landmass[2–4] or in rare cases recycle back into the Earth's mantle via subduction. Known examples of oceanic plateau subduction include the Cretaceous Caribbean Plateau, accreting at and subducting/underthrusting beneath the Greater Antilles on the Caribbean Plate and the south-eastern part of the Ontong Java Plateau presently subducting beneath the Solomon Islands at the north Solomon–Kilinailau trench. Both examples involve complex tectonic processes, such as impact-related accretion of oceanic plateau crust and the change of subduction polarity[5–8]. However, subduction of one tectonic plate beneath another has driven geochemical cycling and the formation of the Earth's crust since ~3,500 Myr[9]. It has been known for decades that volcanic arcs are the result of that subduction process, as the descending plate dehydrates, causing partial melting in the overlying mantle. Consequently, arc lavas carry geochemical signals from the subducting plate, which includes the sediment cover, altered oceanic crust and serpentinized mantle[10–12]. In addition, signals of subducting intraplate seamounts (or LIPs) with geochemical compositions different to the subarc mantle can be traced in arc lavas[13,14]. Tracing the subduction cycle of such geological features provides an improved understanding of mantle-flow pattern and may explain the variability in eruptive behaviour and style of hydrothermal activity on the overriding plate[15].

A globally unique example of single polarity oceanic plateau subduction is the Hikurangi Plateau presently subducting beneath the southern Kermadec arc and the North Island of New Zealand (Fig. 1)[16–19]. Subduction of 15–23-km thick, altered and buoyant Hikurangi Plateau crust, that is host to large seamounts[19,20], must not only have a strong effect on tectonic erosion and the local plate stress regime, but also on volatile element budgets in the overlying mantle. This in turn suggests significant implications for the petrogenesis and eruptive behaviour of arc volcanoes, fluid-flow in their associated hydrothermal systems, and element transfer to the oceans. The Hikurangi Plateau is believed to have formed as part of Ontong Java Nui during the 'greater Ontong Java event' ~120 Myr ago, one of the world's most extreme volcanic events, covering ~1% of the Earth's surface[18,21,22]. As noted by Chandler et al.[22], a large part of the Hikurangi Plateau connecting its western and northern margin with the Ontong Java and Manihiki plateaus either does not exist or has already been subducted.

In this study we present new Sr-, Nd-, and Pb-isotope data from Kermadec arc and Hikurangi Plateau lavas (Fig. 1) which, when combined with published isotope and satellite gravity data and bathymetry, show large-scale geochemical and geophysical variations along the length of the Kermadec arc, enabling us to better understand the processes related to LIP subduction and thus identifying the 'missing' piece of Ontong Java Nui.

Results

Geological background. The ~1,300-km long, intra-oceanic, mostly submarine Kermadec arc system results from Pacific–Australian Plate convergence and forms the southern part of the Tonga–Kermadec arc system that extends ~2,500 km north of New Zealand. The Kermadec arc is one of the worlds most volcanically and hydrothermally active arc systems, with ~75% of the 33 major volcanoes being hydrothermally active[15]. Subduction velocities decrease from the fastest convergence rates on Earth of ~24 cm per year at the northern end of the Tonga arc system[23], to ~5 cm per year along the southern Kermadec arc. The sediment veneer on the incoming Pacific Plate, changes in thickness and
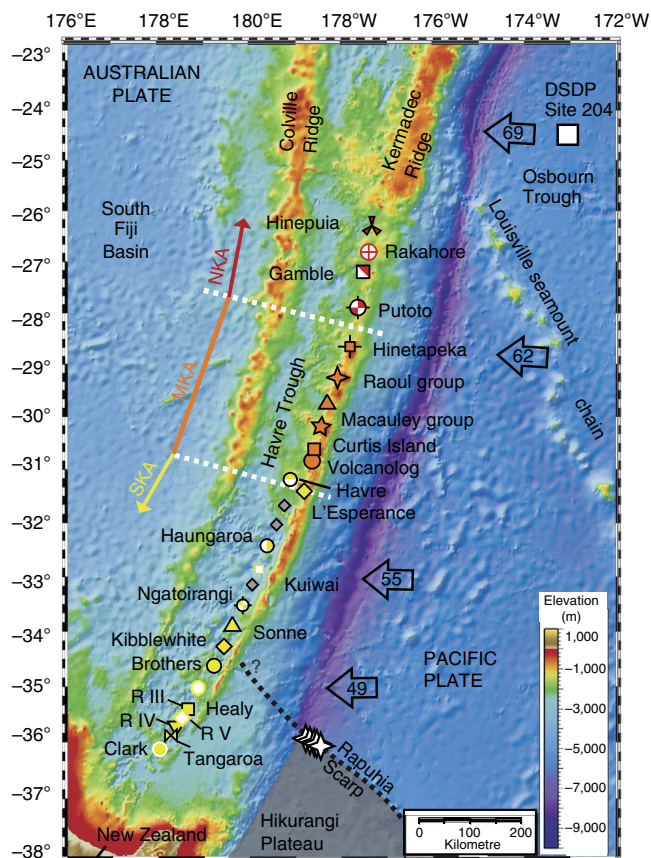

Figure 1 | Bathymetric map of the Kermadec arc—Havre Trough backarc system. Symbols mark the Kermadec arc volcanic centre locations discussed in this paper, with coloured symbols used for the different volcanic centres from which isotopic data are available; the grey symbols are for volcanoes for which no isotope data are available. White stars mark the location of additional Hikurangi Plateau samples used in this study. The numbers in the arrows are subduction velocities, as in ref. 23. For the purpose of this study we separate the Kermadec arc into three segments on the basis of the location of the volcanic front behind or on the Kermadec Ridge: (1) the northern Kermadec arc (NKA) between ~25° and 28.5°S, (2) the mid Kermadec arc (MKA) between ~29 and ~32°S and (3) the southern Kermadec arc (SKA) between 32° and 37°S. DSDP, Deep Sea Drilling Programme.

composition from ~200 m of pelagic sediments near ~25°S (that is, DSDP Site 204; for example, ref. 24; Fig. 1) to ≥500 m of predominantly terrigeneous sediments near ~36°S (ref. 25).

North of ~28.5°S, the Kermadec arc front volcanoes are located in the Havre Trough backarc immediately west of the relatively old and inactive Kermadec Ridge before they merge with the Kermadec Ridge between ~29°S and ~32°S. At ~32°S, the arc front shows a sudden ~15 km offset into the Havre Trough accompanied by ~500 m average seafloor deepening[15,26]. South of 32°S, the majority of the volcanic front volcanoes are located behind the Kermadec Ridge and the forearc narrows by ~75 km from a gently trenchward dipping and ~200-km wide to ~125-km wide[27]. These authors also inferred a westward trench retreat of ≤50 km, and that the forearc inner trench margin south of 32°S subsided by ≤4 km, summing up to a loss in volume of ~400 km³ compared with the north.

South of ~35°S, subduction of the Cretaceous Hikurangi Plateau beneath the southern Kermadec arc is accompanied by an average shoaling of ~500 m of the Kermadec forearc, arc front and Havre Trough backarc[15,28,29]. The plateau hosts ≤2,900 m

high ridge-like seamounts and guyots with basal diameters ≤ 25 km. Two-dimensional gravity modelling and estimates from active seismic source refraction studies suggests a Hikurangi Plateau crustal thickness of 15–23 km compared with a 4–6 km thick Pacific oceanic crust to the north[18,30,31]. Both these techniques assume that the mantle is marked by either Vp seismic velocities > 8 km s^{-1} or densities $> 3.0 \times 10^3$ kg m^{-3}. Reyners et al.[20] however identified a seismically active 35-km thick layer beneath the upper surface of the subducting Hikurangi Plateau. The presence of > 8.5 km s^{-1} velocities at the base of the seismically active zone led Reyners et al.[20] to propose an eclogite layer to the plateau 'crust', doubling the thickness modelled by Davy et al.[18] and Scherwarth et al.[30]

Geochemistry. Lava compositions from the Kermadec arc volcanoes range from basalt to rhyolite within the low-K tholeiitic to medium-K calcalkaline series (e.g. refs 29,32), following the rock classification by Le Maitre[33] and show typical subduction zone enrichments of elements mobile in aqueous fluids (for example, Rb, Ba, U, Pb, Sr) and depletions in Nb when compared with mid-ocean ridge basalts (MORB[34]). Of all the Kermadec arc front lavas, those from the northern Kermadec arc volcanoes between 26 and 28°S show the least radiogenic values for Pb and Sr (for example, ^{206}Pb/^{204}Pb$_{Avg}$ = 18.67; ^{87}Sr/^{86}Sr$_{Avg}$ = 0.7034; see Table 1 for Sr-, Nd- and Pb-isotope data) and fall between Pacific MORB and sediments drilled at DSDP Site 204 (refs 24,35; Fig. 2a,c). The northern Kermadec arc lavas are also characterized

Table 1 | Sr–Nd–Pb-isotope data from selected Kermadec arc volcanic centres and the Rapuhia Scarp of the Hikurangi Plateau

Sample number	Volcano	Rock-type	Latitude	Longitude	Water depth (m)	^{87}Sr/^{86}Sr	^{143}Nd/^{144}Nd	^{206}Pb/^{204}Pb	^{207}Pb/^{204}Pb	^{208}Pb/^{204}Pb
Kermadec Arc volcanic centres										
P72388*	Hinepuia	B	26.41°S	177.28°W	945	0.703369	0.513069	18.697	15.575	38.374
P72356	Hinepuia	A	26.40°S	177.25°W	358	0.703464	0.513071	18.708	15.571	38.384
P72391	Hinepuia	D	26.41°S	177.28°W	945	0.703576	0.513071	18.701	15.574	38.387
P72358	Hinepuia	D	26.40°S	177.25°W	358	0.703529	0.513074	18.709	15.572	38.387
P72403	Hinepuia	R	26.39°S	177.28°W	953	0.703569	0.513066	18.701	15.570	38.374
P72360	Hinepuia	A	26.40°S	177.25°W	358	0.703417	0.513054	18.703	15.573	38.393
P72404	Hinepuia	R	26.39°S	177.28°W	953	0.703418	0.513041	18.592	15.579	38.280
P72428	Rakahore	D	26.81°S	177.40°W	1,053	0.703408	0.513121	18.657	15.573	38.369
P72442	Rakahore	R	26.84°S	177.43°W	690	0.703368	0.513086	18.690	15.576	38.393
P72422	Rakahore	D	26.81°S	177.41°W	786	0.703388	0.513075	18.693	15.575	38.393
P72461	Gamble	R	27.21°S	177.44°W	328	0.703437	0.513106	18.661	15.577	38.381
P72462	Gamble	R	27.21°S	177.44°W	328	0.703423	0.513116	18.660	15.577	38.379
P72448	Gamble	R	27.20°S	177.41°W	620	0.703735	0.513097	18.654	15.574	38.368
P72467	Putoto	B	27.91°S	177.61°W	316	0.703475	0.513110	18.667	15.576	38.369
P72476	Putoto	BA	27.85°S	177.61°W	580	0.703405	0.513096	18.666	15.576	38.355
P72479	Putoto	D	27.85°S	177.61°W	580	0.703478	0.513104	18.660	15.572	38.348
P72483	Putoto	BA	27.85°S	177.61°W	580	0.703431	0.513101	18.661	15.571	38.350
P72490	Putoto	B	27.85°S	177.61°W	580	0.703369	0.513093	18.621	15.566	38.308
P72495	Hinetapeka	D	28.59°S	177.82°W	634	0.703767	0.513064	18.682	15.571	38.436
P72498	Hinetapeka	BA	28.59°S	177.82°W	634	0.703742	0.513037	18.681	15.574	38.432
P72506	Hinetapeka	A	28.65°S	177.80°W	348	0.703771	0.513068	18.683	15.572	38.436
P72511	Hinetapeka	BA	28.65°S	177.81°W	330	0.703776	0.513072	18.688	15.578	38.446
P72497	Hinetapeka	D	28.59°S	177.82°W	890	0.703744	0.513065	18.682	15.572	38.442
T 46-03†	Havre	B	31.09°S	179.06°W	941	0.703708	—	18.757	15.597	38.556
T 51-01	Havre	D	31.14°S	179.01°W	956	0.703707	0.512990	18.770	15.604	38.594
T 34-01	Haungaroa	BA	32.62°S	179.67°W	815	0.703909	0.513013	18.923	15.614	38.717
T 37-03	Haungaroa	B	32.60°S	179.64°W	1,167	0.703889	0.513031	18.934	15.617	38.733
T 27-04	Kuiwai	BA	33.16°S	179.96°W	640	0.703813	—	18.938	15.623	38.758
T 20-02	Ngatoir.	BA	33.74°S	179.83°W	555	0.703906	0.513057	18.867	15.616	38.701
T 24-08	Ngatoir.	BA	33.75°S	179.81°W	1,500	0.703896	0.513140	18.860	15.611	38.687
T 09-01	Sonne	D	34.07°S	179.59°W	1,040	0.703971	0.513012	18.862	15.632	38.737
T 88-01	Sonne	BA	34.02°S	179.56°W	1,271	0.703956	—	18.850	15.614	38.675
T 90-01	Sonne	B	34.08°S	179.48°W	2,405	0.703898	0.512944	18.848	15.614	38.672
T 91-04	Sonne	B	34.12°S	179.43°W	1,841	0.704296	0.512834	18.862	15.640	38.750
T 05-01	Kibblew.	D	34.57°S	179.27°E	1,174	0.703777	0.512949	18.832	15.611	38.638
T 94-02	Kibblew.	B	34.29°S	179.24°E	1,438	0.703246	0.513031	18.788	15.585	38.522
T 98-02	Kibblew.	B	34.69°S	179.30°E	1,642	0.703955	0.513012	18.869	15.607	38.610
Hikurangi Plateau‡										
34-1	RS	B	35.99°S	178.52°W	5,918	0.705057	0.512964	*19.171*	*15.543*	*38.384*
34-4§	RS	B	35.99°S	178.52°W	5,918	0.704586	*0.512954*	19.546	15.574	38.405
34-11	RS	G	35.99°S	178.52°W	5,918	*0.704208*	*0.512945*	19.680	15.550	38.445
36-1§	RS	B	36.03°S	178.28°W	6,001	0.705308	0.512821	18.578	15.531	38.149
36-4	RS	Do	36.03°S	178.28°W	6,001	0.703742	0.512925	19.372	15.634	38.757
38-1§	RS	B	36.12°S	178.39°W	5,868	0.705477	*0.512908*	18.757	15.617	38.520
38-3§	RS	G	36.12°S	178.39°W	5,868	*0.703924*	*0.512927*	19.313	15.600	38.423

B, Basalt; BA, Basaltic Andesite; D, Dacite; Do, Dolerite; G, Gabbro; Kibblew., Kibblewhite; Ngatoir., Ngatoirangi; R, Rhyolite.
*Samples recovered during NZAPLUME III and analysed at the University of Melbourne.
†Samples recovered during TAN0205 and analysed at GEOMAR.
‡Samples recovered during SO168 and analysed at GEOMAR.
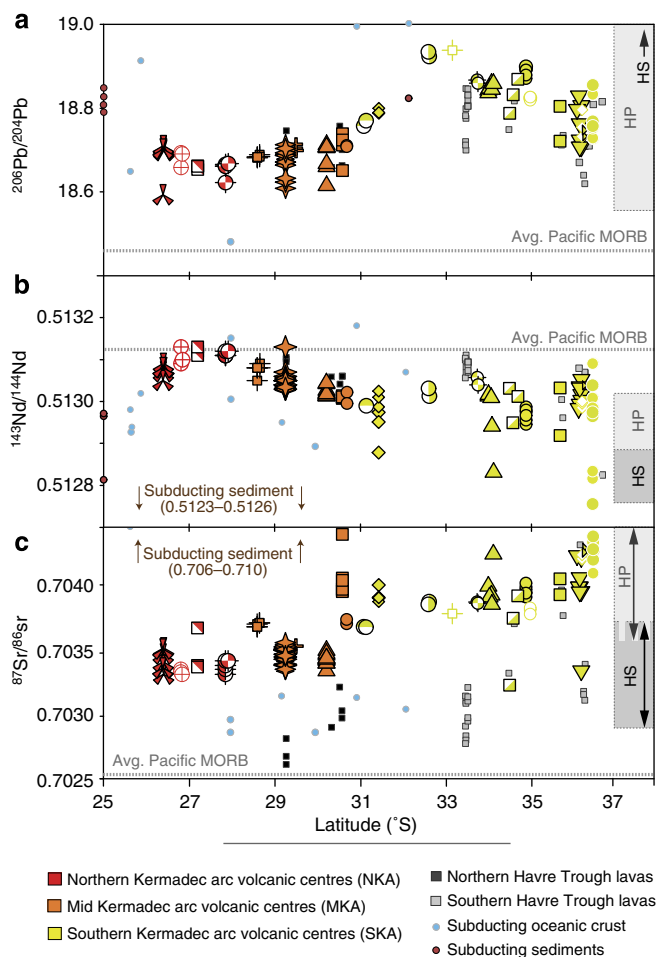§Pb double spike; values in *Italics* from Hoernle et al.[19]

Figure 2 | Isotopic changes with latitude. Latitude (in °S) versus (**a**) $^{206}Pb/^{204}Pb$, (**b**) $^{143}Nd/^{144}Nd$, (**c**) $^{87}Sr/^{86}Sr$. Yellow symbols mark analyses from southern Kermadec arc (SKA) lavas. Orange symbols represent mid Kermadec arc (MKA) lava analyses and red symbols represent northern Kermadec arc (NKA) lava analyses. HP, Hikurangi Plateau and HS, Hikurangi seamounts (data range as in refs 17,19 and this study). Average (avg.) Pacific MORB data are from ref. 55 and references therein. Published Kermadec arc lava data are from refs 24,34–37,56–60. Subducting sediment data are taken from refs 24,35,36,56. Altered oceanic crust data are from refs 61,62. As discussed in ref. 63, the Pb-isotope data set as in ref. 24 were affected by analytical artefacts leading to lower $^{206}Pb/^{204}Pb$ values outside of the analytical error compared with new analyses on the same samples, and thus were omitted in this compilation.

by Pacific MORB-like (most radiogenic) Nd isotopic compositions ($^{143}Nd/^{144}Nd_{Avg} = 0.5131$; Fig. 2b). A noticeable increase in average Pb and Sr isotopic composition to $^{206}Pb/^{204}Pb_{Avg} = 18.69$ and $^{87}Sr/^{86}Sr_{Avg} = 0.7036$, and a decrease in $^{143}Nd/^{144}Nd_{Avg}$ to 0.51304, is shown by lavas erupted on the Kermadec Ridge. At ~32°S, the arc front lava Pb and Sr isotopic compositions become significantly more radiogenic, yet Nd isotope ratios become less radiogenic (for example, $^{206}Pb/^{204}Pb_{Avg} = 18.84$; $^{87}Sr/^{86}Sr_{Avg} = 0.7039$; $^{143}Nd/^{144}Nd_{Avg} = 0.512987$). South of ~35°S above the presently subducting Hikurangi Plateau, the average Pb-isotope composition is variable but on average slightly less radiogenic than in lavas from adjacent volcanoes further north (for example, $^{206}Pb/^{204}Pb_{Avg} = 18.77$), together with slightly higher Sr ($^{87}Sr/^{86}Sr_{Avg} = 0.7042$) and Nd isotope ratios ($^{143}Nd/^{144}Nd_{Avg} = 0.512988$; Fig. 2).

Discussion

Most lavas from the Kermadec arc volcanic centres show MORB-like less fluid mobile and conservative trace element ratios, but generally high element ratios tracing slab-derived fluids (La/Yb < 1; Ba/Th < 1,200; refs 24,34). The Sr and Pb isotopic composition of the northern Kermadec arc lavas have previously been interpreted to show the effects of a MORB-type mantle wedge with the addition of ~1–4% subducted sediment- and altered oceanic crust-derived, fluid-transported isotope signature. Conversely, mantle wedge heterogeneity has been proposed to explain the variations in much less fluid-mobile Nd isotope ratios in northern and southern Kermadec arc lavas[34,36–38]. The generally elevated Sr and Pb, and slightly lower Nd isotope ratios in lavas from mid Kermadec arc volcanic centres located on the Kermadec Ridge have been attributed to (1) the interaction of ascending magmas with older Kermadec Ridge crust with higher Pb and Sr, but lower Nd isotopic values compared with the Havre Trough backarc crust[35,37] and (2) the input of slab-derived fluids carrying more radiogenic Pb and Sr isotope signatures[34]. Despite their emplacement behind the Kermadec Ridge on Havre Trough backarc crust, the southern Kermadec arc lavas also show elevated Pb and Sr, and low Nd isotopic compositions suggesting an isotopically enriched source beneath these volcanoes. Previously, the increase in Pb and Sr isotope ratios in the southern Kermadec arc lavas were considered to be the result of radiogenic New Zealand-derived terrigenous sediment subduction[37]. However, some lavas between ~32–35°S show higher $^{206}Pb/^{204}Pb$ values than local subducting sediment Pb-isotope compositions (Figs 2a and 3c,d), requiring an additional high value $^{206}Pb/^{204}Pb$ component contributing to the arc lava geochemical compositions. One possible endmember is the nearby subducting Hikurangi Plateau with its large HIMU-type (HIMU = high-time integrated U/Pb ratio) seamounts (*cf.* refs 17,19). Exposure of the ~1-km high Rapuhia Scarp (and deep reaching faults on the Hikurangi Plateau[18]) and a ≥1.5-km thick layer of sediments/volcaniclastics to seawater alteration for ~120 Myr suggests that parts of the Hikurangi Plateau are more H_2O-rich than 'normal' altered oceanic crust (supported by high and variable contents of large ion lithophile elements[17,19]).

However, if projected beneath the arc, the Rapuhia Scarp subducts approximately beneath the Kibblewhite volcanic centre (~34.2°S; Fig. 1). Subduction of an H_2O-rich, buoyant and thus shallow dipping Hikurangi slab (~20° to ~60 km depth[39]) is consistent with ~500 m shallowing of the bathymetry, suggesting crustal uplift directly north of Kibblewhite (*cf.* ref. 15). A more buoyant slab, which hosts bathymetric anomalies (such as LIPs) reducing the overall slab density and thus leading to shallow subduction, has also been predicted by numerical models[40]. The colocated change of the arc lava isotope composition, forearc subsidence, arc front offset into the backarc and deepening seafloor morphology together indicate that the initial Hikurangi Plateau–arc collision could have occurred ~250 km further north near ~32°S (refs 15,27).

Supporting evidence for initial Hikurangi subduction ~250 km further north comes from a satellite-derived Bouguer gravity anomaly of up to ~360 mGal between 32°S and 34.5°S, compared with a regional value of ~240 mGal north and south of the anomaly (Fig. 4a), suggesting shallow mantle, or dense mid-lower crust, occurs beneath this region. Two-dimensional gravity modelling along a transect parallel to the Kermadec arc front, from ~30°S to ~35.2°S, indicates maximum crustal thinning at ~32.5°S, gradually thickening both to the north and south from this point. This region of crustal thinning coincides with deeper (by ≤500 m) bathymetry (Figs 1 and 4b). The subduction of major ridges or seamounts is one of the most effective mechanisms to increase tectonic erosion[41]. We can therefore
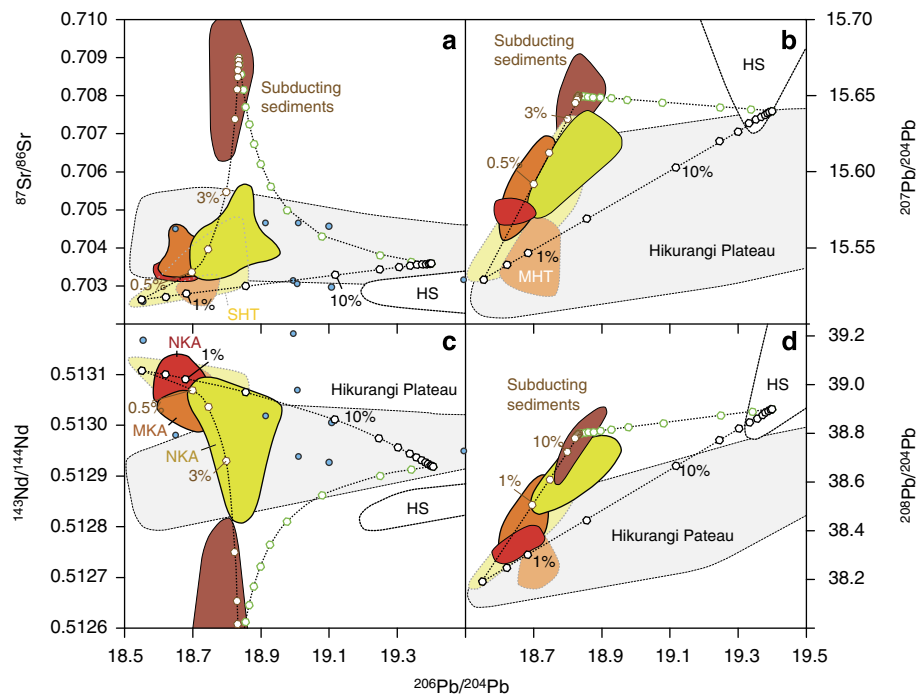
Figure 3 | Kermadec arc Isotopic variation. $^{206}Pb/^{204}Pb$ versus a) $^{87}Sr/^{86}Sr$, b) $^{207}Pb/^{204}Pb$, c) $^{143}Nd/^{144}Nd$ and d) $^{208}Pb/^{204}Pb$. Fields shown are for NKA (red), MKA (orange) and SKA (yellow), subducted sediments (red-brown), Hikurangi Plateau (HP; grey) and Hikurangi seamounts (HS; white); MHT, mid Havre Trough; SHT, southern Havre Trough. Dashed lines with hexagons are mixing calculations between; (1) depleted mantle wedge and subducted sediments, (2) depleted mantle wedge and Hikurangi Plateau (consisting of 90% average Hikurangi Plateau basement and 10% average Hikurangi seamounts) and (3) subducted sediments and Hikurangi Plateau. See Supplementary Table 1 for modelling details. Hikurangi Plateau and seamount data are from refs 17,19, and this study.

assume that the subduction of thickened plateau crust, hosting large seamounts, will significantly increase the rate of tectonic erosion. Much of the margin collapse following removal of plateau support accompanying southward migration of the plateau subduction interface will also enhance effective tectonic erosion[27]. These effects will cause crustal thinning in addition to normal tectonic erosion resulting in the formation of a thick subduction channel mélange at the slab–mantle wedge interface. The apparent increase in crustal thickness towards the south from c. 32.5°, implied by the two-dimensional gravity model (cf. Fig. 4), is likely instead to be partly attributable to dynamic support of the margin (particularly south of 34°) by the subducting buoyant Hikurangi Plateau. Moving southward there is a gradual decrease in the spacing of volcanic edifices along-strike, from one edifice every ~55 km north of ~32°S, to one edifice every ~45 km between ~32° to 35°S and finally to one edifice every ~30 km south of 35°S above the present-day subducting Hikurangi Plateau (cf. ref. 15). This decrease in spacing between volcanic centres is accompanied by an increase in the total volume of lava erupted onto the seafloor from ~830 km³ between 34°S and 32°S to ~1,200 km³ between ~35°S and 37°S (ref. 29), suggesting not only a relation between Hikurangi Plateau subduction and enhanced magma production, but also an impact on the stress field. That is, enhanced fracturing of the overlying plate, creating relatively more zones of weakness, such as faults in the crust along which magmas are channelled and can rise towards the surface. Dehydration of 15–23-km thick and more H_2O-rich Hikurangi crust will significantly increase the fluid flux from the subducting plate, thus forming a more hydrated overlying mantle wedge than to the north.

Erosion of thickened Hikurangi crust and seamounts and subducted sediments will create a buoyant, H_2O-rich 'Hikurangi

mélange', containing a mixture of Hikurangi Plateau basement and seamount material embedded in a metasedimentary matrix including fragments of the overlying crust (cf. Fig. 5). Using a Hikurangi Plateau isotopic composition of $^{206}Pb/^{204}Pb = 19.35$; $^{207}Pb/^{204}Pb = 15.62$; $^{208}Pb/^{204}Pb = 38.74$; $^{87}Sr/^{86}Sr = 0.7037$ and $^{143}Nd/^{144}Nd = 0.51295$ (see Fig. 3 caption for details), the Pb and Sr isotope signatures in lavas from volcanoes located between ~32 and 35°S can be explained by mixing depleted mantle wedge melts with ~3–10% of subducted sediment and ~20–55% Hikurangi components (Fig. 3). Given that the Kermadec arc is one of the oldest and coldest subduction zones globally with an estimated slab surface temperature of ~745–760 °C beneath ~30.2 to 37.9°S (refs 37,42), it is unlikely that significant slab melting will occur. Therefore, although Pb and Sr are mobile in aqueous fluids, the decrease in $^{143}Nd/^{144}Nd$ values cannot be explained through a subducting slab-derived fluid flux alone (due to low Nd mobility in aqueous fluids at temperatures ≤800° (at 4 GPa; ref. 43). Previously, variations in trace element ratios and isotope compositions of rather conservative elements in southern Kermadec arc lavas were attributed to ambient mantle heterogeneity predating the geochemical imprint of the subducting slab[36]. Although ambient mantle wedge heterogeneities (and/or the involvement of deep crustal or lithospheric mantle fragments of rifted Gondwana continental material) could account for the observed isotopic Kermadec arc lava heterogeneities, the simultaneous increase in Pb and Sr but decrease in Nd isotope values, together with the aforementioned observations, plausibly argues for Hikurangi Plateau subduction-related processes causing the observed isotopic changes south of ~32°S. A similar input of an OIB-type slab signature, including a positive gravity anomaly (GH2; Fig. 4a) can be observed further north, where the subduction of the Louisville Seamount Chain affects the central Tonga–Kermadec arc[14].
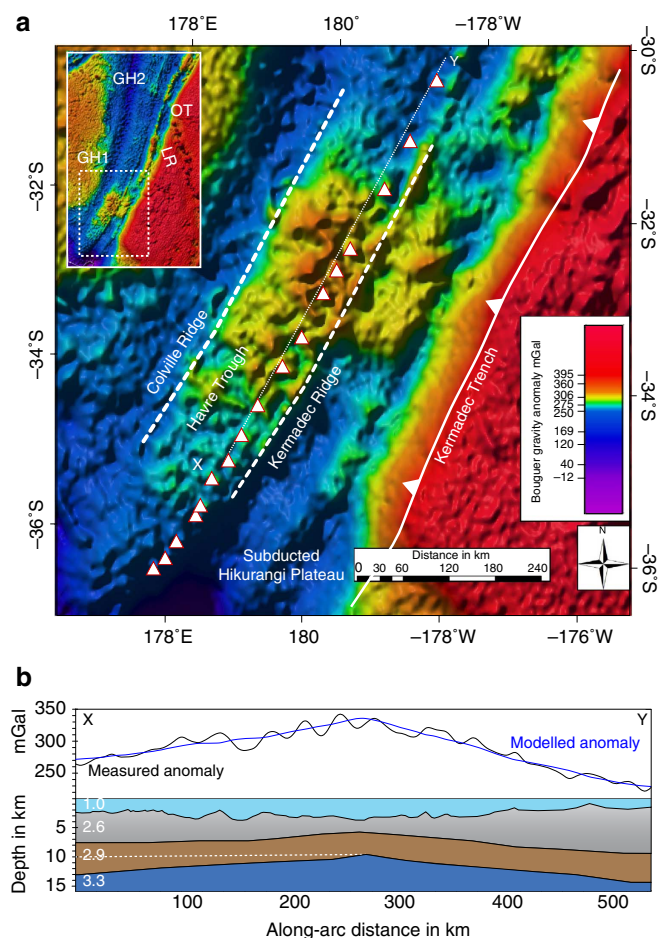
Figure 4 | Bouguer gravity anomaly map and two-dimensional gravity model along the Kermadec arc front. (**a**) Satellite-altimetry-derived Bouguer gravity anomaly map of the Kermadec arc system between ~30°S and ~36.5°S. Bouguer gravity anomaly is calculated using free air gravity anomaly (ref. 64, version 18) plus NIWA bathymetry[65] and a 2.67×10^3 kg m^{-3} density for the water body. Upper left corner inset shows the Bouguer gravity anomaly for the entire arc. Triangles mark the location of the arc front volcanic centres. White dashed line marks the location of the along-arc profile shown in Fig. 4b with X and Y being the start and end points. GH1, gravity high 1; GH2, gravity high 2 (located where the Louisville seamount chain subducts); LSC, Louisville seamount chain; OT, Osbourn trough. (**b**) Two-dimensional gravity model along the Kermadec arc front. Dark blue represents the upper mantle overlain by lower crust (brown), upper crust (grey) and seawater (light blue). White numbers are densities in g cm^{-3}. White dashed line within the lower crust marks hypothetical crustal thickness, assuming the addition of dynamic support of the crust from the buoyant Hikurangi Plateau.

Tomography results from a trench-perpendicular ocean bottom seismometer array oriented east-west across the Kermadec trench to the Havre Trough at ~37°S (refs 30,31) show zones of reduced seismic velocities (that is, Vp ≤ 7.8 km s^{-1} compared with ≥ 8 km s^{-1} for mantle peridotite) beneath the arc front MOHO, consistent with $\geq 10\%$ of serpentenized mantle being present beneath the arc[44]. A similar ~10-km thick crust–mantle transition layer with lower seismic velocities (that is, Vp = 7.0–7.7 m s^{-1}) has also been identified beneath the Izu–Bonin–Mariana and Tonga arcs, interpreted to be composed of a mixture of crustal and mantle materials[45,46]. Likewise, beneath the central Taupo Volcanic Zone, a zone of reduced seismic velocities of $\geq$ Vp = 7.4 m s^{-1} (Vp/Vs = ~1.87)
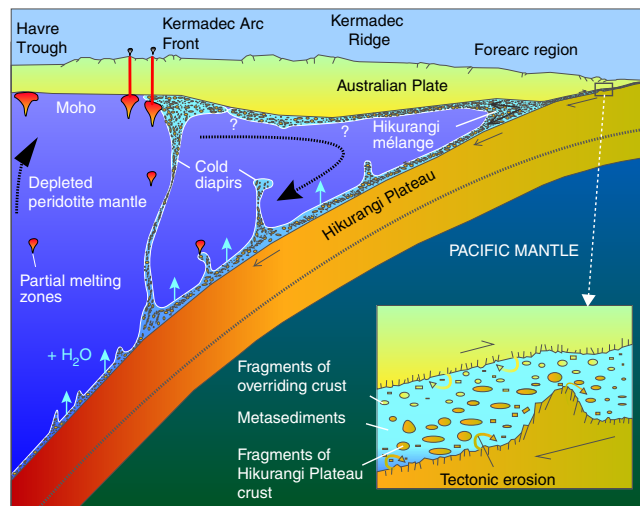
Figure 5 | Schematic across-arc section. Section illustrating the effect of the subducting Hikurangi Plateau on processes in the mantle and crust beneath the southern Kermadec arc. Increased tectonic erosion in the forearc regions creates a thick, H$_2$O-rich mélange layer, containing fragments of the overriding forearc crust and more importantly of the subducting Hikurangi Plateau in a metasedimentary matrix. The Hikurangi mélange is subducted to deeper depth, where due to its buoyant behaviour forms cold diapirs, which rise through mantle wedge and eventually pond beneath a density barrier, such as the Moho. Because of the dehydration of the subducting plate during its descent, the arc lavas may already contain a fluid-derived (mostly Pb and less significant Sr) Hikurangi Plateau signature. Interaction of melts with the Hikurangi mélange layer at the Moho can also explain the large-scale variation of ^{143}Nd/^{144}Nd isotope values not only above the presently subducting Hikurangi Plateau, but also to the north, where the Kermadec arc crust has been underplated in the past. Local variations in lava Sr-, Nd- and Pb-isotope composition may indicate that the Hikurangi mélange does not form a continuous layer beneath the Moho and may only occur locally consistent with its formation through cold diapirs.

extends from the Moho to the slab–mantle wedge interface suggesting diapirically rising hydrated and low density material[47]. Lower seismic velocities of Vp = ~7.7, (and density = ~3.0 g cm^{-3}; Vp/Vs = ~1.85), which are similar to the velocities observed at the crust–mantle boundary beneath arcs have been measured in exhumed subduction mélange rocks with compositions intermediate between chlorite schists and jadeite (at T = 600 °C and P = 2 GPa). Numerical modelling results show that buoyant cold diapir formation requires ~1–10-km thick mélange layers at the slab surface–mantle wedge interface (refs 48,49 and references therein). The formation of a more hydrated Hikurangi mélange above the subducting plateau than beneath the northern Kermadec arc will reduce the mélange density. This, in turn, is likely to create more diapirs rising through mantle wedge and to partially melt via decompression (Fig. 5). The formation of volatile-rich melts above the subducting Hikurangi Plateau can therefore explain the higher volcano density and possibly the formation of large silicic magma chambers beneath the Taupo Volcanic Zone on the North Island of New Zealand (cf. ref. 50). The thin crust between 32 and 34.5°S coincides with the occurrence of large volcanoes, lavas from which show the highest Pb isotopic values, suggesting a high percentage of a Hikurangi component in the mélange formed through increased tectonic erosion during early Hikurangi Plateau subduction. The increasing crustal thickness, ^{87}Sr/^{86}Sr and ^{143}Nd/^{144}Nd values but general decrease of ^{206}Pb/^{204}Pb south
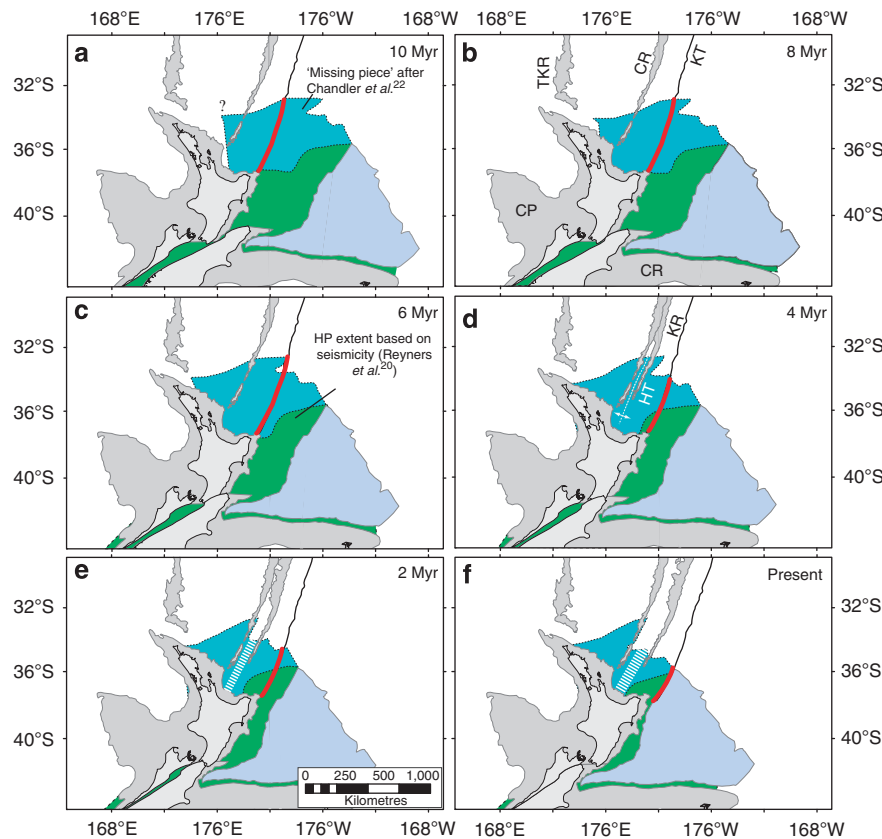
Figure 6 | GPlates-based reconstruction of Pacific and Australian plates NE of New Zealand. Pacific and Australian Plate (Australian Plate fixed and rigid; Kermadec trench fixed) convergence along the Kermadec arc segment are shown in 2 Myr steps from 10 Myr (**a**) to present (**f**) using finite rotations from refs 5,66. CP, Challenger Plateau; CR, Chatham Rise; CR, Colville Ridge; HT, Havre Trough; KR, Kermadec Ridge; TKR, Three Kings Ridge. Dark grey areas represent seafloor above ~2,000 m.b.s.l. Red line in each panel indicates the length of Kermadec Trench beneath which Hikurangi Plateau is subducting. Dashed white line marks the Havre Trough. Present extent of the Hikurangi Plateau (light blue shading), present subducted extent derived from seismic tomography and earthquake hypocentres[20] (green shading), and 'missing piece' of Ontong Java Nui (dark blue shading) from ref. 22. The reconstruction was conducted using GPlates software available at http://www.gplates.org/.

of ~35°S indicates the increasing contribution of a sedimentary component gradually diluting the Hikurangi signature.

We conclude that a geochemically heterogeneous Hikurangi mélange layer, assimilated by younger ascending, or stagnated Kermadec arc melts, can explain the observed change in arc lava geochemical compositions of the southern Kermadec arc lavas. On the basis of isotopic, bathymetric and gravity variations along the Kermadec arc, the initial arc–Hikurangi Plateau collision can be identified at least 250 km north of its present location, suggesting that a much larger portion of the plateau than previously estimated has been subducted since >10 Myr (Fig. 6). The extent of the gap of the Ontong Java Nui super plateau[22] and of the subducted Hikurangi Plateau portion (inferred by geochemistry, morphology and gravity; Fig. 5) suggests that we may have identified the missing piece of this super plateau. Furthermore, we have demonstrated that LIP subduction has profound implications for fundamental processes occurring at oceanic arcs, such as increased rates of tectonic erosion and elevated fluid flux from the subducting slab, which in turn, influence the eruptive behaviour and possibly the style of hydrothermal systems at arc volcanoes and the element transfer into the world's oceans.

Methods

Sampling. The Kermadec arc volcanic centres between ~26°S and 28.6°S (Hinepuia–Hinetapeka) and between ~31°S and 34°S (Havre–Kibblewhite; Fig. 1) were mapped and sampled during the RV Tangaroa expeditions NZAPLUME III

in 2004 and TAN0205 in 2005 (refs 26,33). Additional samples from the Hikurangi Plateau (Rapuhia Scarp) were recovered during the R/V *Sonne* expedition SO168 Zealandia in 2002/2003.

Isotope analyses. For chemical analysis fresh cores of the samples were extracted, repeatedly washed in deionized water (in an ultrasonic bath) to remove sea salt, then crushed, handpicked and reduced to powder in an agate mill. Isotope analyses were conducted at the University of Melbourne and GEOMAR. At the University of Melbourne between 50 and 100 mg of fresh, clean chips 1–5 mm in diameter were handpicked for isotopic analysis and then leached in hot 6 N HCl for 30 min to remove any contaminants. Samples were then washed in ultrapure water and dissolved in HF/HNO$_3$ acid mixtures. Separation of Pb, Sr and Nd involved standard ion exchange procedures using Eichron ion specific resins. Analytical blanks are in all cases insignificant relative to the amount of sample processed and no blank corrections were made. Separated Sr, Nd, and Pb were run on a Nu Instruments MC-ICPMS coupled to a CETAC Aridus desolvating nebulizer operating at a sample uptake rate of ~60 µl min^{-1}. Instrumental mass bias was corrected using an exponential bias law with ^{87}Sr/^{86}Sr normalized to ^{86}Sr/^{88}Sr = 0.1194 and reported relative to NIST SRM 987 = 0.710250. For Sr-isotopes, internal precision is typically <0.000015 (2 s.e.) with reproducibility (2 s.d. of repeat runs) ≤ ±0.000040. ^{143}Nd/^{144}Nd was normalized to ^{146}Nd/^{145}Nd = 2.0719425 (equivalent to ^{146}Nd/^{144}Nd = 0.7219) and reported relative to La Jolla Nd reference material = 0.511865. Internal precision is typically <0.000010 (2 s.e.) with reproducibility (2 s.d. of repeat runs) ≤ ±0.000020. Pb-isotope ratios are reported relative to SRM 981 values of 16.935, 15.489, 36.701 with reproducibility (2 s.d. of repeat runs) ≤ ±0.03%. See refs 51,52 for Pb and Sr–Nd procedures, respectively.

At GEOMAR, leached whole rock powders (6 N HCl at 130 °C for 1 h) were used for Sr, Nd chemistry and leached rock chips (2 N HCl at room temperature for 30 min) for Pb. Sample dissolution involved 4 ml conc. Hf and 1.5 ml HNO$_3$ at 150 °C for 48 h in a closed teflon vial, followed by evaporation to dryness, uptake in 6 N HCl and final evaporation to dryness. The element chromatography followed

established standard procedures[53]. Isotopic ratios were analysed in static multi-collection mode on a TRITON (Nd) and MAT262 RPQ^{2+} (Sr–Pb) thermal ionization mass spectrometers. Sr and Nd isotopic ratios are normalized within run to $^{86}Sr/^{88}Sr = 0.1194$ and $^{146}Nd/^{144}Nd = 0.7219$, respectively and isotope data reported relative to NBS987 $^{87}Sr/^{86}Sr = 0.710250 \pm 0.000012$ (2 s.d., $N = 20$) and $^{143}Nd/^{144}Nd = 0.511850 \pm 0.000005$ (2 s.d., $N = 27$) for La Jolla. NBS981 gave $^{206}Pb/^{204}Pb = 16.898 \pm 0.006$, $^{207}Pb/^{204}Pb = 15.437 \pm 0.007$, $^{208}Pb/^{204}Pb = 36.527 \pm 0.024$ (2 s.d., $N = 125$; 2003–2006) and were corrected for mass bias to our NBS981 double spike values of $^{206}Pb/^{204}Pb = 16.9412 \pm 0.0021$, $^{207}Pb/^{204}Pb = 15.4992 \pm 0.0020$, $^{208}Pb/^{204}Pb = 36.7225 \pm 0.0049$ (2 s.d., $N = 69$; 2006–2008). This external mass bias procedure applies to samples 34-11 and 36-4 while the remaining samples were mass bias corrected by Pb double spike[54]. Total chemistry were <100 ng Sr–Nd–Pb and thus considered neglible relative to the amount of sample.

References

1. Self, S., Jay, A. E., Woddowson, M. & Keszthelyi, L. P. Correlation of the Deccan and Rajahmundry trap lavas: are these the longest and largest lava flows on earth? *J. Volcanol. Geoth. Res.* **99**, 24,275–24,300 (2008).
2. Ben-Avraham, Z., Nur, A., Jomes, D. & Cox, A. Continental accretion: from oceanic plateaus to allochtonous terranes. *Science* **213**, 47–54 (1981).
3. Coffin, M. F. & Eldholm, O. Large igneous provinces: crustal structure, dimensions, and external consequences. *Rev. Geophys.* **32**, 1–36 (1994).
4. Kerr, A. in *Treatise of Geochemistry* (eds Holland, H. & Turekian, K.) 2nd edn, Vol. 4 The Crust (Elsevier, Amsterdam 631–667, 2014).
5. Yan, C. & Kroenke, L. in *Proc. Ocean Drilling Program Scient. Results 130*, 697–709 (Ocean Drilling Program, College Station, TX, 1993).
6. Van der Hilst, R. & Mann, P. Tectonic implications of tomographic images of subducted lithosphere beneath northwestern South America. *Geology* **22**, 451–454 (1994).
7. Mann, P. & Taira, A. Global tectonic significance of the Solomon Islands and Ontong Java Plateau convergent zone. *Tectonophysics* **389**, 137–190 (2004).
8. Hastie, A. R. *et al.* Do Cenozoic analogues support a plate tectonic origin for the Earth's earliest continental crust? *Geology* **38**, 495–498 (2010).
9. de Wit, M. J. *et al.* Formation of an Archean continent. *Nature* **357**, 553–562 (1992).
10. Pearce, J. A. & Peate, D. W. Tectonic implications of the composition of volcanic arc magmas. *Annu. Rev. Earth Planet. Sci.* **23**, 251–285 (1995).
11. Elliott, T., Plank, T., Zindler, A., White, W. & Bourdon, B. Element transport from slab to volcanic front at the Mariana arc. *J. Geophys. Res.* **102**, 14991–15019 (1997).
12. Stern, R. J. Subduction zones. *Rev. Geophys.* **40**, 1012 (2002).
13. Hoernle, K. A. *et al.* Arc-parallel flow in the mantle wedge beneath Costa Rica and Nicaragua. *Nature* **451**, 1094–1098 (2008).
14. Timm, C. *et al.* Louisville seamount subduction and its implication on mantle flow beneath the central Tonga-Kermadec arc. *Nat. Commun.* **4**, 1720 (2013).
15. de Ronde, C. E. J. *et al.* Submarine hydrothermal activity along the mid-Kermadec Arc, New Zealand: large-scale effects on venting. *Geochem. Geophys. Geosys.* **8**, Q07007 (2007).
16. Davy, B. & Wood, R. Gravity and magnetic modelling of the Hikurangi Plateau. *Mar. Geol.* **118**, 139–151 (1994).
17. Mortimer, N. & Parkinson, D. Hikurangi Plateau: a large igneous province in the southwest Pacific Ocean. *J. Geophys. Res.* **101**, 687–696 (1996).
18. Davy, B., Hoernle, K. & Werner, R. Hikurangi Plateau: Crustal structure, rifted formation, and Gondwana subduction history. *Geochem. Geophys. Geosys.* **9**, Q07004 (2008).
19. Hoernle, K. *et al.* Age and geochemistry of volcanic rocks from the Hikurangi and Manihiki oceanic Plateaus. *Geochim. Cosmochim. Acta* **74**, 7196–7219 (2010).
20. Reyners, M., Eberhart-Phillips, D. & Bannister, S. Tracking repeated subduction of the Hikurangi Plateau beneath New Zealand. *Earth Planet. Sci. Lett.* **311**, 165–171 (2011).
21. Taylor, B. The single largest oceanic plateau: Ontong Java–Manihiki–Hikurangi. *Earth Planet. Sci. Lett.* **241**, 372–380 (2006).
22. Chandler, M. T. *et al.* Reconstructing Ontong Java Nui: implications for Pacific absolute plate motion, hotspot drift and true polar wander. *Earth Planet. Sci. Lett.* **331–332**, 140–151 (2012).
23. DeMets, C., Gordon, R. G., Argus, D. F. & Stein, S. Effect of recent revisions to the geomagnetic reversal time scale and estimates of current plate motions. *Geophys. Res. Lett.* **21**, 2191–2194 (1994).
24. Turner, S. P. *et al.* Uranium-238/ thorium-230 disequilibria, magma petrogenesis, and flux rates beneath the depleted Tonga-Kermadec island arc. *Geochim. Cosmochim. Acta* **61**, 4855–4884 (1997).
25. Carter, L., Carter, R. M., McCave, I. N. & Gamble, J. Regional sediment recycling in the abyssal Southwest Pacific Ocean. *Geology* **24**, 735–738 (1996).
26. Collot, J.-Y. & Davy, B. Forearc structures and tectonic regimes at the oblique subduction zone between the Hikurangi Plateau and the southern Kermadec margin. *J. Geophys. Res.* **103**, 623–650 (1998).
27. Davy, B. & Collot, J.-Y. The Rapuhia scarp (northern Hikurangi Plateau)-its nature and subduction effects on the Kermadec Trench. *Tectonophysics* **328**, 269–295 (2000).
28. Collot, J.-Y. *et al.* From oblique subduction to intra-continental transpression: structures of the southern Hikurangi margin from multibeam bathymetry, side scan sonar and seismic reflection. *Mar. Geophys. Res.* **18**, 357–381 (1996).
29. Wright, I. C., Worthington, T. J. & Gamble, J. A. New multibeam mapping and geochemistry of the 30°–35°S sector, and overview, of the southern Kermadec arc volcanism. *J. Volcanol. Geoth. Res.* **149**, 263–296 (2006).
30. Scherwarth, M. *et al.* Fore-arc deformation at the northern Hikurangi margin, New Zealand. *J. Geophys. Res.* **115**, B06408 (2010).
31. Bassett, D. *et al.* Three-dimensional velocity structure of the northern Hikurangi margin, Raukumara, New Zealand: implications for the growth of continental crust by subduction erosion and tectonic underplating. *Geochem. Geophys. Geosys.* **11**, Q10013 (2010).
32. Graham, I. J. *et al.* Structure and petrology of newly discovered volcanic centers in the northern Kermadec-southern Tofua arc, South Pacific Ocean. *J. Geophys. Res. B* **113**, B08S02 (2008).
33. Le Maitre, R. W. in *Igneous Rocks: A Classification and Glossary of Terms, Recommendations of the International Union of Geological Sciences, Subcommission of the Systematics of Igneous Rocks* (eds Streckeisen, A. *et al.*) (Cambridge Univ. Press, 2002).
34. Haase, K. M., Worthington, T. J., Stoffers, P., Garbe-Schoenberg, D. & Wright, I. Mantle dynamics, element recycling, and magma genesis beneath the Kermadec Arc-Havre Trough. *Geochem. Geophys. Geosys.* **3**, 1071 (2002).
35. Ewart, A., Collerson, K. D., Regelous, M., Wendt, J. I. & Niu, Y. Geochemical evolution within the Tonga-Kermadec-Lau arc-back-arc systems; the role of varying mantle wedge composition in space and time. *J. Petrol.* **39**, 331–368 (1998).
36. Todd, E. *et al.* Sources of constructional cross-chain volcanism in the southern Havre Trough: New insights from the HFSE and REE concentration and isotope systematics. *Geochem. Geophys. Geosys.* **11**, 4 (2010).
37. Todd, E. *et al.* Hf isotopic evidence for small-scale heterogeneity in the mode of mantle wedge enrichment: Southern Havre Trough and South Fiji Basin back arcs. *Geochem. Geophys. Geosys.* **12**, Q09011 (2011).
38. Timm, C., Graham, I. J., de Ronde, C. E. J., Leybourne, M. I. & Woodhead, J. Geochemical evolution of Monowai volcanic center: New insights into the northern Kermadec arc subduction system, SW Pacific. *Geochem. Geophys. Geosys.* **12** Q0AF01 (2011).
39. Isacks, B. L. & Barazangi, M. in *Island Arcs Deep Sea Trenches and Back-Arc Basins: Maurice Ewing Ser* (eds Taiwani, M. & Pitman, III W. C.vol. 1 pp. 99–114 (American Geophysical Union, Washington D. C., 1977).
40. Van Hunen, J., van den Berg, A. P. & Vlaar, N. J. On the role of subducting oceanic plateaus in the development of shallow flat subduction. *Tectonophysics* **352**, 317–333 (2002).
41. Ranero, C. R. & von Huene, R. Subduction erosion along the Middle American convergent margin. *Nature* **404**, 748–752 (2000).
42. Syracuse, E. M., van Keken, P. E. & Abers, G. A. The global range of subduction zone thermal models. *Phys. Earth Planet. Int.* **183**, 73–90 (2010).
43. Kessel, R., Schmidt, M. W., Ulmer, P. & Pettke, T. Trace element signature of subductionzone fluids, melts and supercritical liquids at 120-180 km depth. *Nature* **437**, 724–727 (2005).
44. Carlson, R. L. & Miller, D. J. Mantle wedge water contents estimated from seismic velocities in partially serpentinized peridotites. *Geophys. Res. Lett.* **30**, 1250 (2003).
45. Crawford, W. C., Hildebrand, J. A., Dorman, L. M., Webb, S. C. & Wiens, D. A. Tonga Ridge and Lau Basin crustal structure from seismic refraction data. *J. Geophys. Res.* **108**, 2195 (2003).
46. Takahashi, N. *et al.* Structural variations of arc crusts and rifted margins in the southern Izu-Ogasawara arc-back-arc system. *Geochem. Geophys. Geosys.* **10**, Q09X08 (2009).
47. Reyners, M., Eberhart-Phillips, Stuart, G. & Nishimura, Y. Imaging subduction from the trench to 300 km depth beneath the central North Island, New Zealand, with V_p and V_p/V_s. *Geophys. J. Int.* **165**, 565–583 (2006).
48. Gerya, T. V. in *Intra-oceanic subduction zones* (eds Brown, D. & Ryan, P. D.) 23–51 (Arc-Continent Collision, Frontiers in Earth Sciences, 2011).
49. Marschall, H. R. & Schumacher, J. C. Arc magmas sourced from mélange diapirs in subduction zones. *Nat. Geosci.* **5**, 862–867 (2012).
50. Wilson, C. J. N., Gravely, D. M., Leonard, G. S. & Rowland, J. V. in *Studies in Volcanology: The legacy of George Walker Special Publications of IAVCEI* (eds Thordarson *et al.*) Vol. 2, 225–247 (Geological Society of London, 2008).
51. Woodhead, J. D. A simple method for obtaining highly accurate Pb-isotope data by MC-ICPMS. *J. Anal. Atom. Spectrom.* **17**, 1381–1385 (2002).
52. Hergt, J., Woodhead, J. & Schofield, A. A-type magmatism in the Western Lachlan Fold Belt? A study of granites and rhyolites from the Grampians region, Western Victoria. *Lithos* **97**, 122–139 (2007).
53. Hoernle, K. *et al.* Arc-parallel flow in the mantle wedge beneath Costa Rica and Nicaragua. *Nature* **451**, 1094–1097 (2008).

54. Todt, W., Cliff, R. A., Hanser, A. & Hofmann, A. W. in Basu, A. & Hart, S.) (eds) *Earth Processes: Reading the Isotopic Code (Geophysical Monograph)* (American Geophysical Unionvol 95, 429–437, 1996).

55. Meyzen, C. M. *et al.* Isotopic portrayal of the Earth's upper mantle flow field. *Nature* **444,** 1069–1074 (2007).

56. Gamble, J., Woodhead, J., Wright, I. & Smith, I. Basalt and sediment geochemistry and magma petrogenesis in a transect from oceanic island arc to rifted continental margin arc: the Kermadec-Hikurangi Margin, SW Pacific. *J. Petrol.* **37,** 1523–1546 (1996).

57. Gamble, J. A., Christie, R. H. K., Wright, I. C. & Wysoczanski, R. J. Primitive K-rich magmas from Clark volcano, southern Kermadec arc: a paradox in the K-depth relationship. *Can. Mineral.* **35,** 275–290 (1997).

58. Haase, K. A., Stroncik, N., Garbe-Schoenberg, D. & Stoffers, P. Formation of island arc dacite magmas by extreme crystal fractionation: an example from Brothers Seamount, Kermadec island arc (SW Pacific). *J. Volcanol. Geoth. Res.* **152,** 316–330 (2006).

59. Barker, S. J. *et al.* Geochemistry and petrogenesis of silicic magmas in the intra-oceanic Kermadec arc. *J. Petrol.* **54,** 351–391 (2013).

60. de Ronde, C. E. J. *et al.* The anatomy of a buried submarine hydrothermal system, Clark volcano, Kermadec arc, New Zealand. *Economic Geol.* (in press).

61. Worthington, T. J., Hekinian, R., Stoffers, P., Kuhn, T. & Hauff, F. Osbourn Trough: Structure, geochemistry and implications of a mid-Cretaceous paleaspreading ridge in the South Pacific. *Earth Planet. Sci. Lett.* **245,** 685–701 (2006).

62. Castillo, P. R., Londsdale, P. F., Moran, C. L. & Hawkins, J. W. Geochemistry of mid-Cretaceous Pacific crust being subducted along the Tonga-Kermadec Trench: Implications for the generation of arc lavas. *Lithos* **112,** 87–102 (2009).

63. Turner, S. *et al.* Magma evolution in the primitive, intraoceanic Tonga Arc: rapid petrogenesis of dacites at Fonualei volcano. *J. Petrol.* **53,** 1231–1253 (2012).

64. Sandwell, D. T. & Smith, W. H. F. Marine gravity anomaly from Geosat and ERS 1 satellite altimetry. *J. Geophys. Res. B* **102,** 10,039–10,054 (1997).

65. CANZ. *New Zealand Region Bathymetry. New Zealand Oceanographic Institute Miscellaneous Chart Series 73* (National Institute of Water and Atmosphere Research, Wellington, New Zealand, 1997).

66. Cande, S. C. & Stock, J. Pacific-Antarctic-Australian motion and the formation of the Maquire Plate. *Geophys. J. Int.* **157,** 399–414 (2004).

Acknowledgements

Author contributions

C.T. developed the idea and wrote the manuscript. B.D. introduced gravity concepts and with F.C.-T. performed and checked the gravity model. J.W., K.H., K.A.H. and F.H. performed the analyses of the isotope data and contributed them to the manuscript. H.C.S. performed the plate reconstructions. I.J.G., C.E.J.de.R., D.B., N.M., R.J.W. and J.A.G. contributed to the writing of the manuscript. K.A.H. also helped to develop the idea and contributed to the writing of the manuscript.

Additional information

Supplementary Information accompanies this paper at http://www.nature.com/naturecommunications

Competing financial interests: The authors declare no competing financial interests.

Reprints and permission information is available online at http://npg.nature.com/reprintsandpermissions/

How to cite this article: Timm, C. *et al.* Subduction of the oceanic Hikurangi Plateau and its impact on the Kermadec arc. *Nat. Commun.* 5:4923 doi: 10.1038/ncomms5923 (2014).